Alekseyev V.A. Experimental and computational assessment of kinetic conditions of quartz geothermometer use. *UDC 550.4.02*

Vernadsky Institute of Geochemistry and Analytical Chemistry RAS, Russia, 119991, Moscow, st. Kosygina, 19, alekseyev-v@geokhi.ru

Abstract. Quartz geothermometer (*QG*) allows you to determine the temperature of a geothermal reservoir (*GR*) located at depth by the concentration of SiO_2 in the solution that pours from this reservoir to the surface. An error was made in the initial modeling of *QG* (Rimstidt and Barnes, 1980), which unreasonably expanded the scope of *QG* application. Another disadvantage was ignoring the possibility of precipitation of metastable modifications of silica. To eliminate these shortcomings, a new mathematical modeling of *QG* was performed using the finite difference method and new kinetic data. The reliability of the data was assessed by using them in modeling the slow cooling of the quartz–water system and comparing the simulation results with the experimental results of this process. The best agreement between experiments and calculations was obtained when two-stage SiO_2 deposition was used in calculations, when amorphous silica (*AS*) and other modifications of silica were deposited from solutions supersaturated and unsaturated with respect to *AS*, respectively. The boundary values of the ratio of the deposition surface area to the mass of water (*S/M*) and the rate of rise of the solution (v) are determined, at which the model predicts the correct readings of *QG* for different temperatures of the solution in *GR* and at the surface.

***Keywords**: quartz geothermometer, amorphous silica, mathematical modeling, finite difference method, experiment*

QG measurements are carried out according to the temperature dependence of quartz solubility in water (m_{eq}), assuming an equilibrium concentration of silica in *GR* and maintaining this concentration as the solution rises to the surface. The basis of the *QG* is the silica–water reaction, the rate of which is described by the difference in the rates of dissolution and precipitation of quartz (Rimstidt, Barnes, 1980):

$$dm/dt = (S/M)k_d(1 - m/m_{eq}), \quad (1)$$

where t is the time, and k_d is the quartz dissolution rate constant. In the *QG* model constructed in (Rimstidt and Barnes, 1980), a *GR* with silica-saturated water relative to quartz is located at a depth of 2 km at a temperature of 300°C. Water from the *GR* rises through the pores and cracks of the host rock and cools at the surface to 25°C. Later, we repeated these calculations (Alekseyev, 1997) using the finite difference method with equation (1), the temperature dependences k_d and m_{eq}, and the residence time of the solution (Δt) at the temperature step ΔT:

$$\Delta t = \Delta T/(vg), \quad (2)$$

where g is the temperature gradient. The initial silica concentration at the subsequent temperature step was equal to the final concentration at the previous step. Calculations were performed from 300 to 25°C with a small step ($\Delta T = 0.001°$), which ensured their high accuracy. A comparison of the two calculations revealed their significant discrepancy (Alekseyev, 1997) caused by errors in early modeling. For example, the dotted vertical line on the right in Fig. 1, taken from (Rimstidt and Barnes, 1980) for v = 0.0001 m/s and *S/M* = 1 m^2/kg, shows the consistency of the composition of the solution as it rises from the *GR* to the surface, which means the correct reading of *QG*. However, our calculations using the same equations with the same values of v and *S/M* gave a significantly lower value of m at the surface (left solid curve), which means an incorrect reading of *QG*. To get closer to the correct *QG* reading, you need to increase v by at least 2 orders of magnitude (right solid curve), and in order for the *QG* reading to be correct, you need to increase v by another order of magnitude. After correcting the error, the correct readings of the *QG* were possible only at very low values of *S/M* and at very high values of v. This circumstance significantly narrowed the application scope of the *QG*.

Another disadvantage of early modeling was that it ignored the possibility of precipitation of other silica modifications. The fact is that quartz deposition in the old model is described by equation (1) with the k_d values obtained by dissolving quartz, since the principle of microscopic reversibility of the reaction (1) was assumed to be fulfilled. Later experiments showed that when silica was deposited on quartz seeds, k_d values were 3 orders of magnitude lower (Alekseyev et al., 2009), which means a violation of this principle away from equilibrium. In this case, silica was first deposited in the form of *AS*, which, as the supersaturation of the solution decreased, gradually transformed into more stable modifications of silica: opal-CT, opal-C, quartz. *AS* precipitation instead of quartz also occurs in pipelines of geothermal power plants when the temperature decreases (van den Heuvel et al., 2018), i.e. under conditions of *QG* action. Depending on the mechanism of nucleation (homogeneous or heterogeneous), *AS* can be deposited through polymerization in the volume of the solution or through growth on the surface of the seeds (van den

Heuvel et al., 2018). The heterogeneous mechanism better corresponds to natural conditions, where the solution comes into contact with the walls of pores and cracks, which act as seeds. A number of papers have been published in which the deposition rates of *AS* on seeds have been measured and rate equations have been obtained (Carroll et al., 1998; Faimon, Blecha, 2008). The *Tes* temperature dependence of quartz dissolution rate constant (Fig. 2) has a slightly steeper slope than *RB* line and is probably more accurate because of additional data. However, both dependences were obtained from experiments in which quartz was mostly dissolved. In this study, the *Al* dependence (Fig. 2) may be more appropriate, which is located quite far from the previous dependencies, but describes precisely the deposition of silica onto quartz seeds (Alekseyev et al., 2009). Similar dependencies for *AS*, given in different works, also differ markedly from each other (dotted lines in Fig. 2).

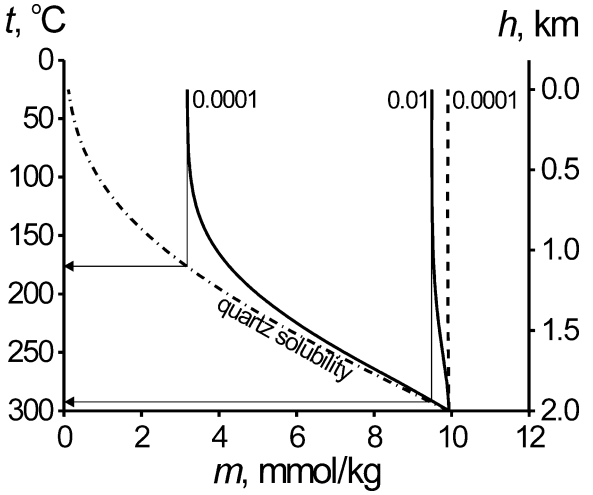

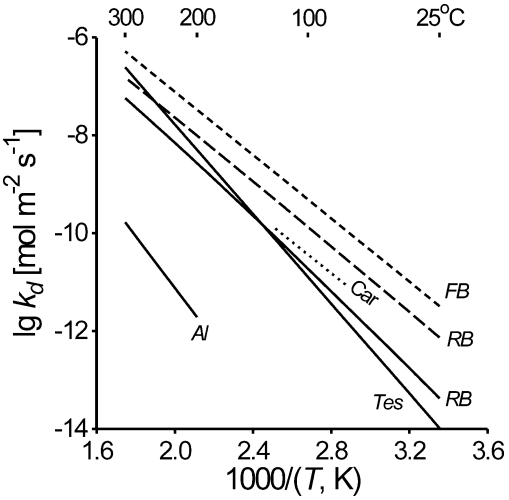

Fig. 1. Quartz geothermometer readings (thin straight lines with arrows) in the model (Rimstidt, Barnes, 1980) for *S/M* =1 m^2/kg at different rates of solution rise (m/s) according to calculations performed in (Rimstidt, Barnes, 1980) (dotted line) and in in this paper (solid lines) using the same equations.

Fig. 2. Temperature dependences of the dissolution rate constant (k_d) of quartz (solid lines) and amorphous silica (dotted line) according to Rimstidt and Barnes, 1980 (*RB*), Tester et al., 1994 (*Tes*), Alekseyev et al., 2009 (*Al*), Faimon, Blecha, 2008 (*FB*), Carroll et al., 1998 (*Car*).

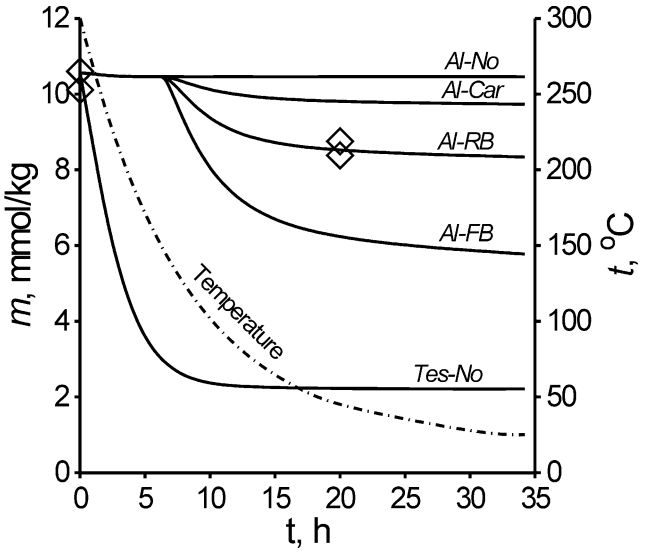

Fig. 3. The change in the SiO_2 concentration in solution (m) over time (t) during cooling of the quartz–water system (*S/M* = 1000 m^2/kg), according to the results of calculations (curves) and experiments (symbols). The calculations used the k_d values for quartz from Tester et al., 1998 (*Tes*) or Alekseyev et al., 2009 (*Al*). The k_d values for amorphous silica were not used (*No*) or were taken from Rimstidt and Barnes, 1980 (*RB*), Carroll et al., 1998 (*Car*), Faimon and Blecha, 2008 (*FB*).

To assess the reliability of these data, experiments were performed with crushed quartz (10-63 microns) purified from fine particles (Alekseyev et al., 2009) and water (*S/M* = 1000 m^2/kg). In these experiments, quartz–water equilibrium was first achieved at 300°C, and then this system was slowly cooled in a switched-off electric furnace, simulating the rise of the solution from a hot *GR* to a cold surface under the action of *QG*. The temperature change in a cooling electric furnace over time is approximated by the equation (Voldek, 1978):

$$t(h) = U\ln[(T_\infty - T)/(T_\infty - T_0)], \quad (3)$$

where U is the time constant (adjustment parameter), T_0 and T are the body temperature at the beginning of cooling (300°C) and at time t, T_∞ is the ambient temperature (21°C). The smallest average square deviation of the calculated and measured temperature values (1.6°) was obtained at U = -8.06. 20 hours after the start of cooling of the electric furnace, when the temperature dropped from 300 to 47°C, the value

of *m* decreased slightly in the experiments (Fig. 3). The *Tes-No* curve, constructed using k_d for quartz from (Tester et al., 1994), when performing the principle of microscopic reversibility of the reaction, turned out to be significantly lower than the experimental values of *m*. The *Al-No* curve, constructed using k_d from (Alekseyev et al., 2009) in violation of this principle (slow precipitation), turned out to be higher than the experimental values of *m*. The best agreement with the experiments was obtained in a two–stage calculation (*Al-RB* curve), where k_d from (Alekseyev et al., 2009) was used before saturation of *AS*, and above that, from (Rimstidt and Barnes, 1980) for *AS*. These kinetic data were used in the subsequent *QG* simulation.

The results of the new simulation depended on *S/M* and *v*, but were the same for the same ratio of these values, since this ratio is included in equation (1), given that the value Δt is related to *v* by expression (2). For this reason, the simulation results (Fig. 4) are shown for different values of $n = \lg[(S/M)/v]$, each of which is a set of pairs of values of *S/M* and *v* with the same ratio to each other. The most complete picture of the change in the composition of the solution is presented in a model with a maximum temperature range from 300 to 25°C (Fig. 4a). At low values of *n* (0-3), the solution does not change its composition as it rises to the surface, i.e. *QG* gives the correct temperature value of *GR*. With an increase of $n > 3$, the calculated curves deviate more and more into the range of lower values of *m*, i.e. the readings of *QG* deviate more and more from the correct value. These deviations are amplified in the low-temperature region, causing the calculated curves to bend due to faster deposition of *AS*. An increase in the final temperature of the solution at the surface from 25 to 100°C (Fig. 4c) did not significantly change the position of the boundary between the correct and incorrect readings of the *QG*. However, a decrease in the initial temperature of the solution in *GR* from 300 to 200°C (Fig. 4b) shifted this boundary to the region of large values of *n* by one, and a simultaneous increase in the final temperature of the solution at the surface from 25 to 100°C (Fig. 4d) shifted this boundary by one more.

The ranges of *S/M* and *v* values, which ensure correct *QG* readings for different models, are summarized in Fig. 5. The maximum value of *v* on the ordinate axis is 1 m/s, which is close to the upper limit of this value in geothermal systems (Okamoto and Tsuchiya, 2009). In the experiments, the cooling rate of the solution varied from 30 to 3 °/h. In the *QG* model in Fig. 3a, these cooling rates correspond to the rise rates of the solution from 0.06 to 0.006 m/s, which is quite realistic for natural conditions.

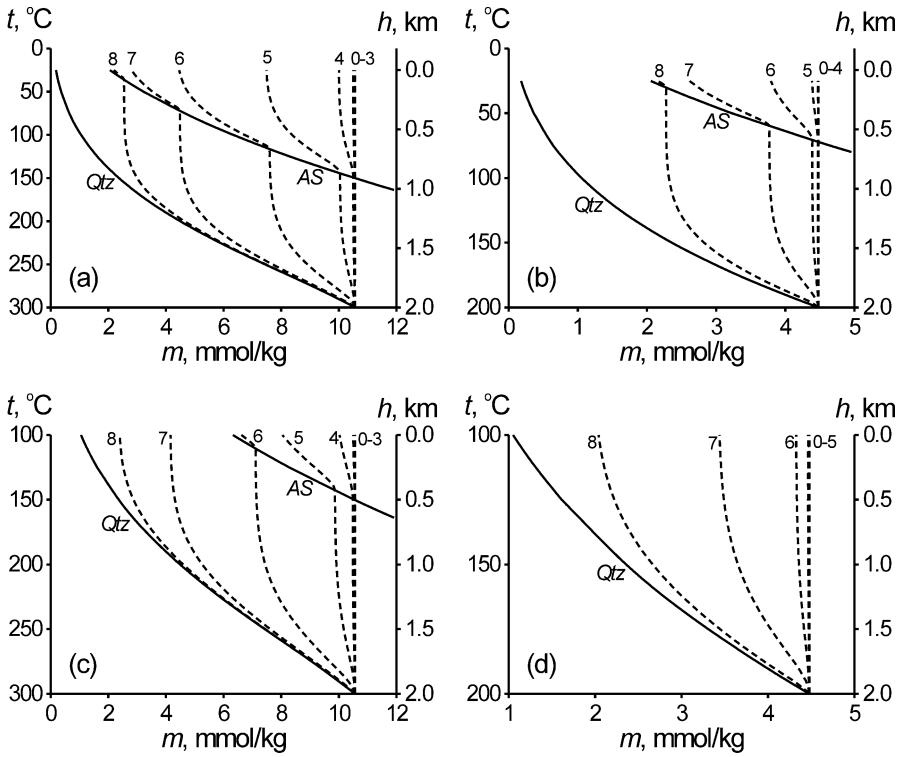

Fig. 4. The change in the concentration of dissolved silica (*m*) when the solution rises from a geothermal reservoir with a temperature of 300 (a, c) or 200°C (b, d) and cools at the surface to 25 (a, b) or 100°C (c, d). The numbers show the values of $n = \lg (S/M, m^2/kg) - \lg (v, m/s)$. The k_d value in calculations between the solubilities of quartz (*Qtz*) and amorphous silica (*AS*) is taken from (Alekseyev et al., 2009), and in solutions supersaturated with respect to *AS*, it is taken for *AS* from (Rimstidt and Barnes, 1980).

The minimum *S/M* value on the abscissa axis (Fig. 5) is 1 m^2/kg, which corresponds to a crack width of 2 mm and is probably close to the lower limit of this value in geothermal systems (Rimstidt and Barnes, 1980). The experimental *S/M* value (1000 m^2/kg) is higher than this value, which also indicates its reality for natural conditions. The new modeling has significantly expanded the scope of the *QG* application compared to the old one (dotted line in Fig. 5).

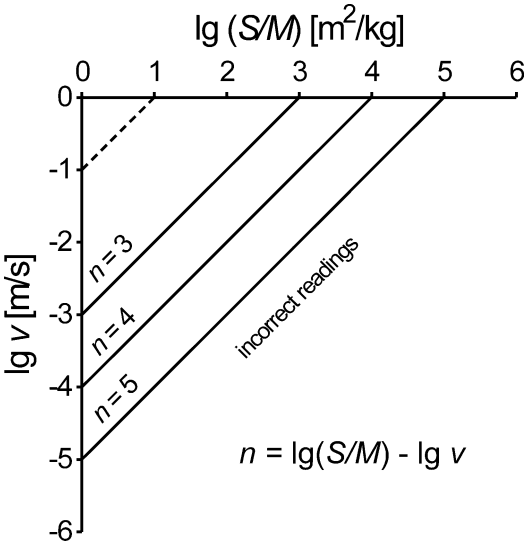

Fig. 5. Boundaries between the areas of correct and incorrect readings of quartz geothermometer in the models shown in Fig. 4. The dotted line shows a similar boundary for the corrected model of Rimstidt and Barnes (1980).

The deposition of *AS* instead of quartz can be explained by the influence of an additional parameter, namely, the smaller size of the critical nucleus due to the lower interphase energy at the mineral–solution interface (Okamoto et al., 2010). The presence of seeds accelerates the deposition of *AS* (Carroll et al., 1998). This means that numerous kinetic studies of homogeneous deposition of *AS* are probably unsuitable for modeling *QG*, a characteristic element of which is the presence of rough crack walls that play the role of seeds and initiate heterogeneous silica deposition.

The rate of precipitation of *AS* depends not only on the degree of supersaturation of the solution, but also on the rate at which this supersaturation is created (Tobler, Benning, 2013), as well as on the pH and Na content in the solution (Bohlmann et al., 1980), and the Al content in *AS* (Carroll et al., 1998). The representation of these dependencies in the form of equations will make it possible in the future to perform more accurate modeling of *QG*, close to real natural processes.

References

Alekseyev V.A. Kinetic characteristics of the Na/K geothermometer operation // Geochem. Int. 1997. Vol. 35. No 11. P. 997-1006.

Alekseyev V.A., Medvedeva L.S., Starshinova N.P. Kinetics of silica precipitation on quartz seeds at 200–300°C // Geochem. Int. 2009. Vol. 47. No 7. P. 731-735.

Bohlmann E.G., Mesmer R.E., Berlinski P. Kinetics of silica deposition from simulated geothermal brines // Soc. Petrol. Eng. J. 1980. Vol. 20. No 04. P. 239-248.

Carroll S., Mroczek E., Alai M., Ebert M. Amorphous silica precipitation (60 to 120°C): Comparison of laboratory and field rates // Geochim. Cosmochim. Acta. 1998. Vol. 62. No 8. P. 1379-1396.

Faimon J., Blecha M. Interaction of freshly precipitated silica gel with aqueous silicic acid solutions under ambient and near neutral pH-conditions: A detailed analysis of linear rate law // Aquat. Geochem. 2008. Vol. 14. No 1. P. 1-40.

Okamoto A., Tsuchiya N. Velocity of vertical fluid ascent within vein-forming fractures // Geology. 2009. Vol. 37. No 6. P. 563-566.

Okamoto A., Saishu H., Hirano N., Tsuchiya N. Mineralogical and textural variation of silica minerals in hydrothermal flow-through experiments: Implications for quartz vein formation // Geochim. Cosmochim. Acta. 2010. Vol. 74. No 13. P. 3692-3706.

Rimstidt J.D., Barnes H.L. The kinetics of silica-water reactions // Geochim. Cosmochim. Acta. 1980. Vol. 44. No 11. P. 1683-1699.

Tester J.W., Worley W.G., Robinson B.A., Grigsby C.O., Feerer J.L. Correlating quartz dissolution kinetics in pure water from 25 to 625°C // Geochim. Cosmochim. Acta. 1994. Vol. 58. No 11. P. 2407-2420.

Tobler D.J., Benning L.G. In situ and time resolved nucleation and growth of silica nanoparticles forming under simulated geothermal conditions // Geochim. Cosmochim. Acta. 2013. Vol. 114. P. 156-168.

van den Heuvel D. B., Gunnlaugsson E., Gunnarsson I., Stawski T., Peacock C. L., Benning L. G. Understanding amorphous silica scaling under well-constrained conditions inside geothermal pipelines // Geothermics. 2018. Vol. 76. P. 231-241.

Voldek A.I. Electric machines. L.: Energiya, 1978. 832 p.

Korzhinskaya V.S. Behavior of sodium and calcium during dissolution of natural pyrochlore in chloride solutions. *UDC 550.814*

Korzhinskii Institute of Experimental Mineralogy RAS (IEM RAS), Chernogolovka, Moscow region (vkor@iem.ac.ru)

Abstract. The experimental results of the behavior of sodium and calcium at dissolution of natural pyrochlore $(Ca,Na)_2$ $(Nb,Ta)_2O_6(O,OH,F)$ in chloride solutions HCl,KCl and NaCl with the concentrations from 0.01m to 2m for temperatures 300°-550°C and pressures 50, 100 MPa in the presence of oxygen buffers Ni-NiO and Co-CoO are represented. It is determined that the number of Ca in the solution increases markedly with the growth of HCl

concentration and reaches the values $n*10^{-5}$ mole/kg H_2O in 0.01m HCl and $n*10^{-2}$ mole/kg H_20 in 2m HCl . In KCl and NaCl solutions, calcium content does not practically change with the growth of chlorides concentration. In all chloride solutions, Na content rises with the growth of chloride concentration. The biggest Na content is discovered in the solutions of NaCl and HCI. In KCl solutions Na content is 3 orders lower. In the presence of the oxygen buffer Ni -NiO , the Ca content in HCl and KCl solutions with a concentration of 0.01 m is an order higher than that for the Co-CoO buffer. For other HCl and KCl concentrations it is lower of less than one order of magnitude. The obtained results point to the incongruent solubility of natural pyrochlorine in chloride solutions with the predominant transition into Na and Ca solution as compared to niobium.

***Keywords**: experiment, solubility, pyrochlore, calcium, sodium, chloride solutions, physico- chemical conditions.*

The data of the investigation continue experimental work on dissolution, transfer and deposit of Ta and Nb minerals by hydrothermal fluids. Earlier we studied columbite-tantalite behavior in fluorine and chloride solutions, what is valid for Ta deposits, related to lime-alkaline, including lithium-fuorine granities (apogranites) (Korzhinskaya and et al., 2014, Zaraisky et al., 2010). The investigations of the behavior of pyrochlore minerals $(Ca, Na)_2(Nb, Ta)_2O_6(O, OH, F)$ and columbite $(Mn,Fe)(Nb,Ta)_2O_6$ in carbonate and alkaline solutions typical for the deposits of Nb and Ta , genetically related to alkaline granites, alkaline sienites and carbonatites are held (Korzhinskaya et al., 2017; Kotova et al., 2024). This paper shows the experimental results of Na and Ca behavior at dissolution of pyrochlore $(Ca, Na)_2Nb, Ta)_2O_6(O, OH, F)$ in chloride solutions of HCl, KCl, NaCl with the concentrations from 0.01m to 2m for temperatures 300 – 550 ^{o} C and pressures 50, 100 MPa in the presence of oxygen buffers Ni-NO and Co-CoO.

For the runs pyrochlore monocrystals from the weathering crusts of the carbonatite deposit Tatarka of the following composition Na_2O-7.61%; CaO-14.28%; Nb_2O_5-71.61%; F-5.18%; TiO_2-0.83%; $Ta_2O_5\leq$ wt./% were taken. The runs lasted 30-15 days. The runs were held in platinum capsules of 10 x0,2x 60 mm in size at a hydrothermal exoclave high pressure vessel. Oxygen buffers Ni -NiO and Co-CoO were placed into the reactor in containers isolated from the weight charge. The quenching solution was analyzed by ICP/MS and ICP/AES (mass-spectral and atomic-emission) methods for a number of elements (Nb, Ta, Ca, Mn, Fe, Ti etc.). To determine a chemical composition of newly-formed phases, X-ray-phase and microprobe analysis methods were used (Cam Scan MV2300 (VE GA TS5130 MM).

The results of the experiments on study of concentration and temperature dependences of equilibrium contents of sodium and calcium at pyrochlore dissolution in the solutions of HCl, KCl and NaCl at T = 300^{o} - 550^{o}C, P = 50 - 100 MPa are given in **Table 1.**

Table 1. Experimental data on solubility of natural pyrochlore in chloride fluids

№ run.	Initial solution, mol/кg H_2O	Na, mol/кg H_2O	Ca, mol/кg H_2O	Nb, mol/кg H_2O
550^{o}C, 100 MPa, buffer Co-CoO				
Px-173	0,01m HCl	2,57E-02	4,49E-05	2,78E-04
Px-169	0,1m HCl	0,127	7,59E-04	7,18E-05
Px-170	1m HCl	0,439	7,55E-02	2,99E-03
Px-178	2m HCl	0,522	3,24E-02	2,60E-03
Px-165	0,01m KCl	1,86E-03	4,03E-05	1,71E-07
Px-166	0,1 KCl	4,96E-03	4,64E-05	5,27E-07
Px-177	1m KCl	2,33E-02	2,50E-05	8,72E-07
Px-167	2m KCl	4,25E-02	2,03E-05	2,18E-06
Px-174	0,01m NaCl	0,103	7,73E-05	1,40E-07
Px-175	0,1m NaCl	8,70E-03	1,77E-04	6,78E-07
Px-176	1m NaCl	0,921	2,50E-04	3,12E-07
Px-172	2m NaCl	2,53	3,78E-04	2,96E-06
Px-213	1m LiCl	0,236	5,24E-04	≤ DL
Px-214	2m LiCl	0,243	4,92E-04	2,48E-06
550^{o}C, 100 MPa, buffer Ni-NiO				
Px-205	0,01mHCl	9,96E-03	3,69E-04	1,40E-06
Px-206	0,1mHCl	0,124	1,74E-03	2,48E-04
Px-207	1m HCl	0,21	0,12	2,07E-03

№ run.	Initial solution, mol/кg H_2O	Na, mol/кg H_2O	Ca, mol/кg H_2O	Nb, mol/кg H_2O
Px-208	2m HCl	0,689	6,49E-02	5,12E-03
Px-209	0,01m KCl	5,35E-03	8,31E-04	6,03E-05
Px-210	0,1m KCl	6,83E-03	1,20E-04	2,15E-06
Px-211	1m KCl	2,75E-02	6,24E-05	3,23E-06
Px-212	2m KCl	3,51E-02	2,22E-04	2,69E-06
400°C, 100 MPa, buffer Co-CoO				
Px-198	1m HCl	0,622	7,99E-02	5,27E-05
Px-197	0,1m HCl	0,108	3,12E-04	1,40E-06
Px-196	0,01m HCl	1,14E-02	1,37E-04	1,08E-07
Px-183	0,01m KCl	1,14E-02	≤ DL	4,74E-07
Px-184	0,1m KCl	1,63E-02	6,79E-05	9,58E-07
Px-185	1m KCl	3,19E-02	≤ DL	1,61E-07
300°C, 100 MPa, buffer Co-CoO				
Px-179	0,01m HCl	1,18E-02	3,24E-05	1,61E-06
Px-180	0,1m HCl	8,30E-02	1,57E-02	1,94E-06
Px-181	1m HCl	9,13E-02	8,96E-02	1,41E-04
Px-182	2m HCl	0,826	0,134	2,48E-05
550°C, 50 MPa, buffer Co-CoO				
Px-203	0,1m HCl	5,16E-02	3,72E-03	5,60E-05
Px-202	1m HCl	0,345	5,03E-02	4,02E-03
Px-201	2m HCl	0,341	2,55E-02	1,88E-03
400°C, 50 MPa, buffer Co-CoO				
Px-192	0,1m HCl	0,179	3,09E-04	4,86E-06
Px-193	1m HCl	0,627	0.113	3,01E-05
Px-194	0,1m KCl	6,61E-03	2,59E-04	2,15E-07
Px-195	1m KCl	1,34E-02	5,06E-03	2,80E-06

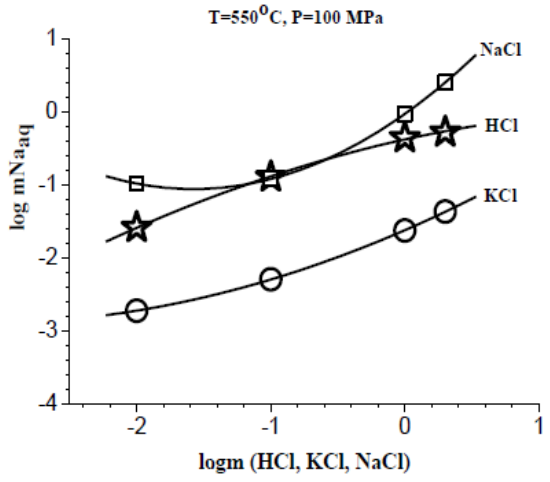

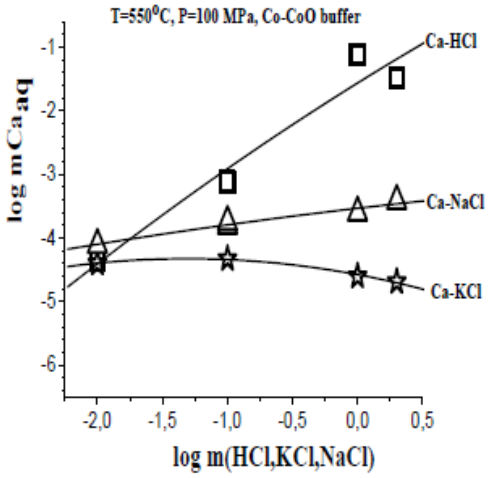

Fig.1. Concentration dependence of sodium content at pyrochlore dissolution in chloride solutions NaCl, HCl, KCl (T = 550°C, P = 100 MPa, buffer Co-CoO).
Fig.2. Concentration dependence of calcium content at pyrochlore dissolution in chloride solutions HCl, NaCl, KCl (T = 550°C, P = 100 MPa, buffer Co-CoO).

Fig.1 shows concentration dependence of sodium content at pyrochlore dissolution in HCl, KCl and NaCl solutions at T= 550°C and P = 100MPa and buffer Co-CoO. Na content in all chloride solutions rises as chloride concentration grows. The largest Na content is discovered in HCl and NaCl solutions (see Table 1}. In KCl solutions Na content is 3 orders of magnitude lower: for 0.01 m KCl It is $1.86*10^{-3}$, for 2m KCl it is $4.25*10^{-2}$ mol/ kg H_2O.

Fig.2 shows concentration dependence of calcium in the solutions HCl, KCl and NaCl at pyrochlore dissolution for T = 550°C and P = 100

MPa and buffer Co-CoO. As HCl concentration grows, equilibrium Ca concentration at pyrochlore dissolution rises and reaches the values $n*10^{-5}$ mol/kg H_2O in 0.01 m HCl and $n*10^{-2}$ mol/kg H_2O in 2m HCl. In KCl and NaCl solutions Ca content does not practically change with the increase of chloride concentration.

Study of the influence of pressure for T = 400°C and P = 50 - 100 MPa on calcium content at pyrochlore dissolution in HCl and KCl solutions is given in **Fig.3**. The experiments showed that in KCL solutions Ca content rises with pressure increase by almost 0.5 -0.7 log. In HCl solutions Ca content has a linear dependence. In this case it changes little with pressure rise.

It is determined that in the region of low concentrations HCl (0.01m) Ca equilibrium content in the presence of the buffer Co-CoO is an order of magnitude lower than that in the presence of the buffer Ni-NiO (**Fig.4**). As the initial HCl concentration grows, to 1 m Ca equilibrium content in the presence of both buffers becomes practically the same. For KCl solutions the similar picture is observed: in the presence of Ni-NiO buffer Ca content in the solution 0.01 m KCl is higher by an order. Then in the region of concentrations (0.1 – 1 m) KCl in the presence of the buffer Ni- NiO. Ca content is a little bit higher (0.5 log).

Concentration dependence of niobium behavior at pyrochlore dissolution in HCl, KCl and NaCl is shown in Fig.5. As we can see from this figure, the increase of the initial concentration HCl from 0.01 m to 2 m results in a small growth of Nb content in the solution by an order of magnitude only. Here m Nb for 0.01 m HCl is $2.75*10^{-4}$, but for 2 m HCl it is $2.63*10^{-3}$ mol/kg H_2O. In the initial solutions KCl and NaCl concentration curves for Nb practically coincide. Here equilibrium Nb content in these solutions is not essential and is $1.40*10^{-7}$ – $1.70*10^{-7}$ mol/kg H_2O in KCl and NaCl solutions, respectively. As the initial KCl and NaCl concentrations grow to 2 m, Nb content increases only by an order of magnitude and for 2 m KCl it is $2.19*10^{-6}$ and for 2 m NaCl it is $2.95*10^{-6}$ mol/kg H_2O.

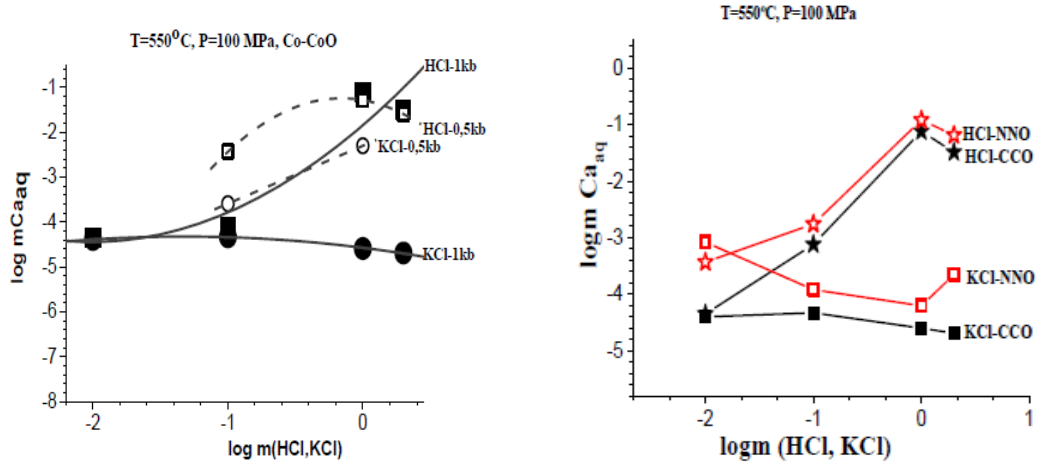

Fig.3. Influence of pressure on calcium content at pyrochlore dissolution in HCl and KCl solutions (400°C, P - 50 and 100 MPa, buffer Co-CoO).
Fig.4. Influence of redox conditions (buffers Co-CoO and Ni-NiO) on equilibrium content of calcium at pyrochlore dissolution in HCl and KCl solutions (T = 550C, P - 100 MPa).

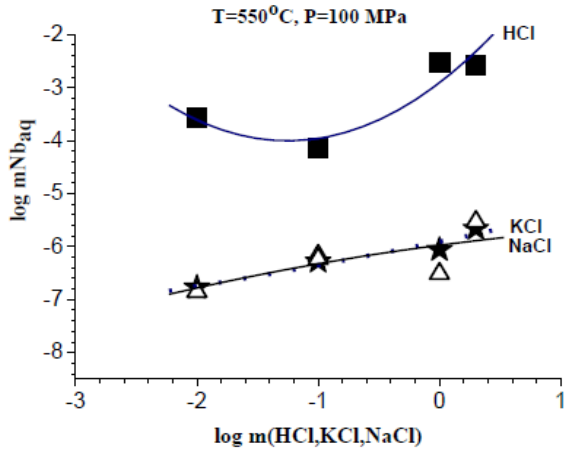

Fig. 5. Concentration dependence of Nb equilibrium content at pyrochlore dissolution in chloride solutions: HCl, KCl, NaCl for T = 550°C, P = 100 MPa (buffer Co-CoO).

The obtained results are sure to show unambiguously incongruent pyrochlore solubility in chloride solutions with a predominant transfer to sodium and calcium solution as compared to niobium. T hus, we can conclude that in chloride solutions saturation on pyrochlore is attained due to high concentration of sodium and calcium in the solution at a much lower niobium solubility.

The work was supported by the FMUF-2022-0003 program.

References

Korzhinskaya V.S., Kotova N. P., Shapovalov Yu. B. Experimental Study of Manganese Tantalite and Ta_2O_5 Solubility in Chloride Solutions // Doklady Earth Sciences. **2014.** V. 459. P.P. 1409–1412.

Kotova N.P., Korzhinskaya V.S., Shapovalov Yu.B. Experimental Study of the Solubility of Columbite, Pyrochlore, and Ta and Nb Oxides in Alkaline Hydrothermal Fluids at 300–550°C and 50 and 100 MPa / Doklady Earth Sciences. **2024.** V.514. №2. P.P. 287-295.

Korzhinskaya V.S., Kotova N.P. Shapovalov Yu.B. Experimental Study of Natural Pyrochlore and Niobium Oxide Solubility in Alkaline Hydrothermal Solutions // Doklady Earth Sciences, 2017. V. 475(1). PP. 793-796.

Zaraisky G.P., Korzhinskaya V.S., Kotova N.P. // J. Mineral and Petrol. 2010. V. 99. № ¾. PP. 287–300.

Kotova N.P., Korzhinskaya V.S. Study of the behavior of natural pyrochlore and niobium oxide in chloride aqueous fluids (based on experimental data).

Korzhinskii Institute of Experimental Mineralogy RAS
kotova@iem.ac.ru, vkor@iem.ac.ru.ac.ru

Abstract. The influence of physicochemical parameters (solution concentration, temperature, pressure, oxidation-reduction conditions) on the solubility of the natural mineral pyrochlore and niobium oxide in model water-salt fluids HCl, KCl, NaCl, LiCl with concentrations of 0.01 – 2 m at 300 – 550 °C, 50 and 100 MPa (buffers Co-CoO and Ni-NiO) was studied. It has been established that in hydrothermal chloride solutions in equilibrium with the indicated minerals, a positive concentration dependence of the niobium content is observed for both pyrochlore and Nb_2O_5. The influence of temperature, fluid pressure and redox conditions on the solubility of Nb_2O_5 and pyrochlore is insignificant. A comparative analysis of the equilibrium Nb contents was carried out when dissolving Nb_2O_5 and pyrochlore in HCl and KCl solutions in the concentration range of 0.01 – 2 m at 550 °C and 100 MPa.

***Keywords**: experiment, solubility, pyrochlore, niobium oxide, fluid, physicochemical conditions*

The study of the distribution of tantalum and niobium between the fluid and magmatic melt in the region of relatively low P and T is of great interest for understanding the problem of the source of these metals and the physicochemical conditions of the genesis of Ta and Nb deposits associated with granitoid and alkaline magmatism (Beus A.A. et al., 1962). Therefore, special experimental studies of the solubility of tantalum-niobates of complex composition (columbite, pyrochlore, etc.), as well as simple oxides of Ta and Nb. in fluoride, chloride, alkaline, carbonate solutions of different concentrations and T-P-fO_2 conditions corresponding to the physicochemical parameters of postmagmatic processes, are of paramount importance (Aksyuk, 2002; Zaraisky et al. 2010; Korzhinskaya et al., 2014; Kotova, 2014).

The influence of physicochemical parameters (solution concentration, temperature, pressure, oxidation-reduction conditions) on the solubility of the natural mineral pyrochlore and niobium oxide in model water-salt fluids HCl, KCl, NaCl, LiCl was studied. In the experiments, fragments of natural pyrochlore single crystals $(Ca, Na)_2(Nb, Ta)_2O_6(O, OH, F)$ from the weathering crusts of the Tatarka carbonatite deposit (composition according to microprobe determinations: Na_2O-7.61%; CaO-14.28%; Nb_2O_5-71.61%; F-5.18%; TiO_2-0.83%; $Ta_2O_5 \leq 1\%$ by weight) and a chemical reagent (β-Nb_2O_5) (special purity grade), which is an analogue of the mineral nioboxide, which is rarely found in nature, were used. The experiments were carried out on a high-pressure hydrothermal installation in welded platinum tubes at 300 – 550° C, P = 50 - 100 MPa under conditions of low oxygen fugacity corresponding to oxygen buffers Co-CoO and Ni-NiO. The concentrations of the solutions varied within the range of 0.01m - 2m. Run duration was 15-30 days.

To control congruent or incongruent dissolution and to determine chemical composition of newly-formed phases (in case of their detection) the initial materials and solid run products were studied by X-ray diffraction, and electron microprobe analysis (Cam Scan MV 2300 (VEGA TS5130MM).

The quenched aqueous solutions were then analyzed using ICP/MS (Inductively Coupled Plasma Mass Spectrometry) and ICP/AES (Atomic Emission Spectroscopy) for Nb, Ta, Mn, and Fe and admixture elements Ti, W, and Sn.

Previously, we discovered a strong negative effect of increasing oxygen fugacity on the solubility of columbite-tantalite in HF and HCl solutions. To determine the influence of oxidation-reduction conditions on the solubility of natural pyrochlore $(Ca, Na)_2(Nb, Ta)_2O_6(O, OH, F)$ in chloride solutions, a series of experiments were carried out in 0.1 and 1 m HCl and KCl solutions at 400 and 550° C and 100 MPa in the presence of solid-phase oxygen

buffers Co-CoO and Ni-NiO. It was found that under reducing conditions (Co-CoO buffer) the solubility of pyrochlore was higher than in the presence of Ni-NiO buffer. All further experiments were carried out in the presence of Co-CoO buffer.

The results of experiments on studying the concentration dependences of the equilibrium content of niobium during the dissolution of niobium oxide and pyrochlore in solutions of HCl, KCl, NaCl and LiCl at T = 550 °C, P = 100 MPa (Co-CoO buffer) are presented in Fig. 1 (a, b).

During the experiments it was found that when dissolving niobium oxide in low concentration HCl solutions, with an increase in the acid concentration, the niobium content in the solution decreases from $10^{-4.8}$ mol/kg H_2O in 0.01 m HCl to $10^{-5.3}$ mol/kg H_2O in 0.1 m HCl, and then with a further increase in the acid concentration it increases, reaching a maximum value of $10^{-3.7}$ mol/kg H_2O in 2 m HCl (Fig. 1a).

In KCl solutions, the trend of change in the solubility of niobium oxide from the concentration of KCl is negative. With an increase in the concentration of potassium chloride, the content of niobium in the solution decreases from $10^{-4.7}$ mol/kg H_2O in 0.01m KCl to $10^{-5.2}$ mol/kg H_2O in 1 m KCl, and then increases slightly to $10^{-4.7}$ mol/kg H_2O in 2 m KCl. Thus, it can be concluded that the solubility of Nb_2O_5 in KCl solutions in the low concentration region is of the same order as in HCl solutions, and in the concentration region of 1 and 2 m it is an order of magnitude lower.

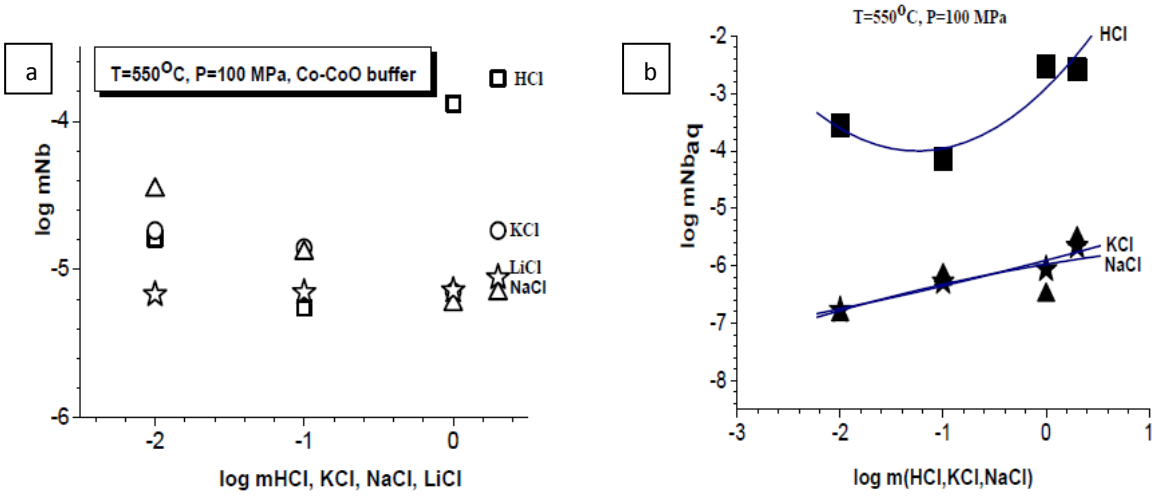

Fig.1(a) Concentration dependence of Nb_2O_5 solubility in chloride solutions (HCl, KCl, NaCl, LiCl) at *T*=550°C, *P*=100МПа (Co-CoO buffer)

Fig.1(b) Concentration dependence of the equilibrium content of niobium during the dissolution of pyrochlore in chloride solutions (HCl, KCl, NaCl) at *T*=550°C, *P*=100МПа (Co-CoO buffer)

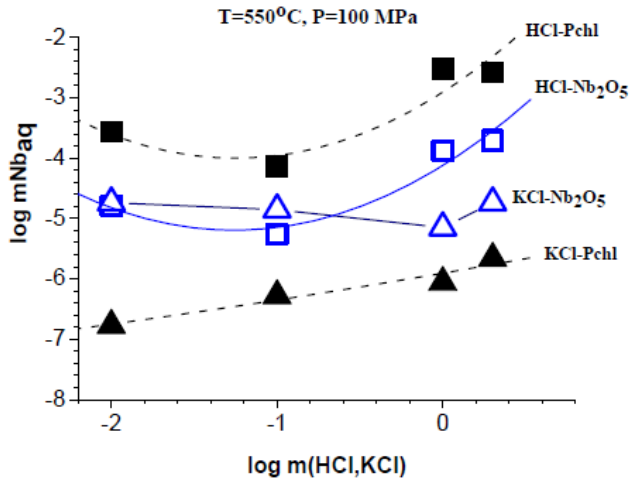

Fig. 2. Concentration dependence of the equilibrium content of niobium during the dissolution of pyrochlore (Pch) and Nb_2O_5 in chloride solutions (HCl, KCl) at *T*=550°C, *P*=100МПа (Co-CoO buffer)

In NaCl solutions, by analogy with KCl solutions, the trend of change in niobium solubility from NaCl concentration is negative. With increasing concentration of sodium chloride, the niobium content in the solution decreases from $10^{-4.5}$ mol/kg H_2O in 0.01m NaCl to $10^{-5.2}$ mol/kg H_2O in 1 m KCl. In 2 m NaCl solution, the niobium content increases by only 0.1order of magnitude, reaching a value of $10^{-5.1}$ mol/kg H_2O.

In LiCl solutions, with an increase in the concentration of lithium chloride, the niobium content remains virtually unchanged, remaining at the same level ($10^{-5.2}$ mol/kg H_2O).

The data from the X-ray phase analysis of solid experimental products clearly prove that in the entire studied range of chloride solution concentrations, niobium oxide dissolves congruently, that is, without changing the composition. The data from the X-ray phase analysis of solid experimental products clearly

prove that in the entire studied range of chloride solution concentrations, niobium oxide dissolves congruently, that is, without changing the composition.

A comparison of the results of experiments on studying the concentration dependences of the equilibrium content of niobium during the dissolution of niobium oxide and pyrochlores in solutions of HCl, KCl, NaCl (Fig. 2) showed that the content of niobium in HCl solutions for the pyrochlore mineral increases with increasing concentration from 10^{-4} in 0.01 m HCl to 10^{-3} mol/kg H_2O in 2 m HCl. Moreover, the niobium content for pyrochlore is more than an order of magnitude higher than for niobium oxide, which can be explained by the high solubility of sodium and calcium present in pyrochlore. The niobium content for pyrochlore increases with increasing KCl concentration and is 10^{-7} for 0.01 m KCl; 10^{-6} mol/kg H_2O for 1 m KCl, but remains three orders of magnitude lower than the solubility in HCl. The solubility of Nb_2O_5 in KCl solutions in the low concentration region is of the same order as for HCl, and in the concentration region of 1 and 2 m it is an order of magnitude lower. But compared to pyrochlore, the solubility of niobium oxide remains 2 orders of magnitude higher in the region of low solution concentrations and one order of magnitude higher for high KCl concentrations. In NaCl solutions, pyrochlore and niobium oxide behave similarly to KCl solutions and have the same order of solubility.

Fig. 3 (a, b) shows the results of studying the temperature dependence of the equilibrium content of niobium during the dissolution of niobium oxide and pyrochlore in HCl solutions of different concentrations at P = 100 MPa (Co-CoO buffer).

Studies have shown that at T = 300°C the equilibrium contents of niobium during the dissolution of niobium oxide in solutions of 0.1 m and 1m HCl coincide (Fig. 3a). When the temperature increases from 300°C to 500°C, the niobium content in a 0.1 m HCl solution increases slightly from $10^{-5.7}$ mol/kg H_2O to $10^{-5.3}$ mol/kg H_2O, remaining at the same low level. n 1 m HCl solutions, with an increase in temperature from 300 to 550°C, the equilibrium content of niobium increases by approximately 1.5 orders of magnitude - from $10^{-5.7}$mol/kg H_2O to $10^{-3.9}$ mol/kg H_2O (Fig. 3a).

The data from the X-ray phase analysis of solid experimental products clearly prove that in the entire studied range of concentrations of chloride solutions of HCl in the entire studied range of temperatures at P = 100 MPa, niobium oxide dissolves congruently, that is, without changing the composition.

During experiments to study the temperature dependence of pyrochlore solubility (Fig. 3b), it was found that when dissolving pyrochlore in HCl solutions of different concentrations (0.01m, 0.1m and 1m) in the temperature range of 300-550 °C and P = 100 MPa, a negative temperature dependence is observed with an increase in temperature from 300 to 400 °C. With a further increase in temperature from 400 °C to 550 °C, an increase in the equilibrium content of niobium in HCl solutions is observed: from 10^{-7} mol / kg H_2O to $10^{-3.5}$ mol / kg H_2O in 0.01m HCl solutions; from $10^{-5/8}$ mol / kg H_2O to 10^{-4} mol/kg H_2O in 0.1m HCl solutions and from $10^{-3/5}$ mol/kg H_2O to $10^{-2.5}$ mol/kg H_2O in 1m HCl solutions.

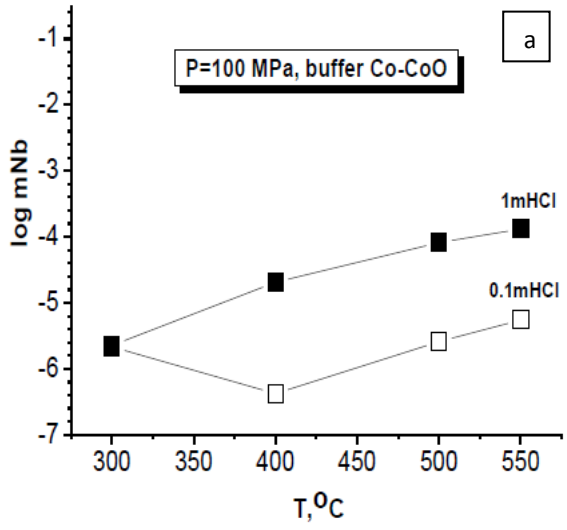

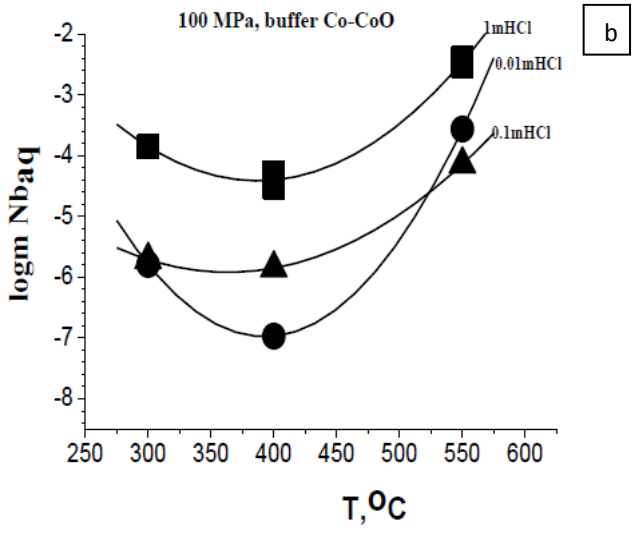

Fig. 3(a) Temperature dependence of the equilibrium content of niobium during the dissolution of Nb_2O_5 in HCl solutions at *P* = 100 МПа (Co-CoO buffer)

Fig. 3(b) Temperature dependence of the equilibrium content of niobium during the dissolution of pyrochlore in HCl solutions at *P* = 100 МПа (Co-CoO buffer)

To determine the effect of pressure on the solubility of pyrochlore and niobium oxide in aqueous chloride fluids HCl and KCl, a series of experiments were carried out at a pressure of 50 and 100 MPa. Analysis of the obtained data on the solubility of niobium oxide in 0.1m HCl solutions at T = 550°C and P = 50, 100 MPa showed that with an increase in pressure from 50 to 100 MPa, the equilibrium content of Nb in 0.1m HCl solutions remains virtually unchanged, remaining at the level of $n*10^{-5.2}$ mol/kg H_2O. In 1m HCl solutions, with an increase in pressure from 50 to 100 MPa, the equilibrium content of Nb increases from $n*10^{-5.2}$ mol/kg H_2O to $n*10^{-3.8}$ -mol/kg H_2O. In 0.1m and 1m KCl solutions, an increase in pressure from 50 to 100 MPa leads to an increase in the equilibrium content of niobium in these solutions from n*10-6 mol/kg H_2O to n*10-5 mol/kg H_2O, respectively.

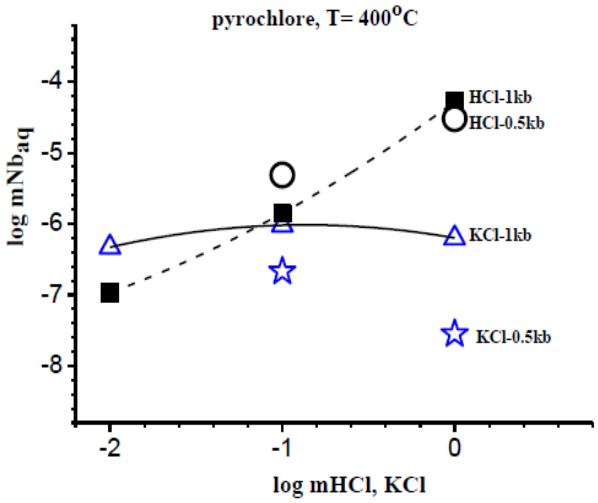

Fig. 4. The influence of HCl, KCl concentration and fluid pressure of 50 and 100 MPa on the solubility of pyrochlore at 400°C (Co-CoO buffer)

The diagram (Fig. 4) shows the results of experiments to study the effect of pressure on the solubility of pyrochlore in 0.1m and 1m solutions of HCl and KCl at T = 400°C and P = 50 and 100 MPa (Co-CoO buffer). It has been established that in HCl solutions the influence of pressure on the solubility of pyrochlore is insignificant. When the pressure increases from 50 to 100 MPa, the increase in the equilibrium content of niobium is only about 0.5 log. In KCl solutions, the increase in niobium content with increasing pressure from 50 to 100 MPa is 0.7 log for 0.1 m KCl and 1.2 log for 1 m KCl.

A comparative analysis of the maximum Nb contents during the dissolution of Nb_2O_5 and pyrochlore in chloride solutions at 550°C and 100 MPa allows us to conclude that in hydrothermal chloride solutions in equilibrium with the indicated minerals, a positive concentration dependence of the niobium content is observed for both pyrochlore and Nb_2O_5. The influence of temperature, fluid pressure and redox conditions on the Nb_2O_5 and pyrochlore solubility is insignificant.

The obtained results clearly prove the incongruent solubility of pyrochlore in chloride solutions with a preferential transition to sodium and calcium solution compared to niobium. On this basis, it can be concluded that in chloride solutions the solubility product (saturation) for pyrochlore is achieved due to the high concentration of sodium and calcium in the solution with a lower solubility of niobium.

The conducted studies allow us to draw a general conclusion that in the entire range of studied conditions, in all chloride solutions, both at low and at high chloride concentrations, the solubility of niobium is low and is within the range of 10^{-5} -10^{-4} m. At such low concentrations, it is difficult to judge the actual mass transfer of niobium by hydrothermal chloride solutions and the possibility of its concentration during the formation of industrial deposits.

The work was carried out with the financial support of the Russian Federation represented by the Ministry of Education and Science of Russia, project No. 13.1902.24.44, agreement No. 075-15-2024-641.

References

1 Aksyuk A.M. Experimentally validated geofluorimeters and fluorine regime in granite fluids // Petrology. 2002. 10. No 6. P. 630-644.

2 Korzhinskaya V.S., Kotova, N.P. and Corresponding Member of the RAS Shapovalov Y.B. Experimental study of Manganese Tantalite and Ta_2O_5 solubility in chloride solutions// Doklady Earth Sciences. 2014. V. 459. No 1. P. 1409-1412

3 Kotova, N.P. Experimental study of Nb_2O_5 solubility in fluoride solutions at T=550°C and P=500 bar // Experimental Geochemistry. 2014. V. 2. No 3. P. 319

4. Beus A.A., Severov E.A., Sitnin A.A., and Subbotin K.D. Albitized and greisenize granites (apogranites) // Akademiia Nauk SSSR. 1962. 196 p. (in Russian).

5. Zaraisky G.P., Korzhinskaya V.S., Kotova N.P. Experimental studies of Ta_2O_5 and columbite-tantalite solubility in fluoride solutions from 300 to 550°C and 50 to 100 MPa // Miner. Petrol. 2010. V. 99. No 3-4. P. 287-300. doi: 10.1007/s00710-010-0112-z.

Novikov M.P., Nekrasov A.N.. Gorbachev P.N. About the genesis of the kularite. *UDC 550.4*

Korzhinskii Institute of Experimental Mineralogy RAS
Chernogolovka, Chernogolovka, Moscow district, Russia
novikovi@chgnet.ru

Abstract. To clarify the genesis of gold-rare earth-phosphate mineralization confined to black shale strata of the North-Eastern rare earth belt, the composition of natural kularite (phosphate of rare earths of the Se subgroup), monazite and rhabdophanite of this region, as well as their synthetic analogues obtained in experiments on synthesis with a full set of all rare earth elements were studied.

Samples containing microconcretions of kularite of three types, differing in the color of grains, are similar in the content of rare earth oxides. As a rule, all the studied samples contain thorium in varying quantities and a direct correlation with SiO_2 is observed, which gives reason to assert the formation of an independent phase of $ThSiO_4$, corresponding to the natural mineral hattonite and crystallizing in the monoclinic syngony, like kularite.

***Keywords**: cularite, hattonite, rare earth orthophosphates, microconcretions, crystal zoning.*

Introduction. Stratiform deposits of many ore metals are subordinate to black shale formations, periodically formed in the sedimentary shell of the Earth, composing vast belts in folded regions. A characteristic feature of such deposits is the absence of a visible spatial connection with intrusive complexes. However, analysis of parageneses of ore metals reveals genetic connections with magmatism, often of a certain type. The discovery of black shale formations with unique gold-rare earth-phosphate (kularite) deposits subordinate to them is the greatest achievement of the present time. The geography and distribution areas of kularite deposits associated with black shale formations are described in the work (Nekrasov, Nekrasova, 1995). Kularite (rare earth orthophosphate of the Se subgroup) was found in large quantities in the Kularsky Ridge in northeastern Yakutia within the Verkhoyansk folded system in Permian and Triassic black shale deposits enriched in phosphate matter (Nekrasova, Nekrasov, 1982). The uniqueness of this deposit is that along with gold mining, there is the possibility of associated extraction of rare earth elements represented by the mineral kularite, isostructural with monazite, which, according to its discoverers, is an authigenic variety. The very name of the mineral still raises controversial issues, but it should be recognized that morphologically it differs significantly from the magmatic monazite of granitoids, isostructural with it (Nekrasova, 1995).

Research methods. For a detailed study of the natural material, we selected three types of kularite varieties, differing in color: gray, dark gray and black. In all cases, kularite is microconcretions in the form of ellipsoid grains no larger than 1 mm (Fig. 1).

Electron probe microanalysis, including obtaining an image of the studied object in secondary and reflected electrons, as well as X-ray spectral local microanalysis, was performed on a Tescan VEGA TS 5130MM (CamScan MV2300) TPPT digital scanning electron microscope equipped with YAG detectors of secondary and reflected electrons and an INCA Energy 350 energy-dispersive X-ray spectrometer with an INCA PENTAFet x3 semiconductor Si (Li) detector. Calculations of the X-ray spectral microanalysis results were performed using the Microanalysis Suite Issue 18d +SP3 (INCA Suite version 4.15) software package.

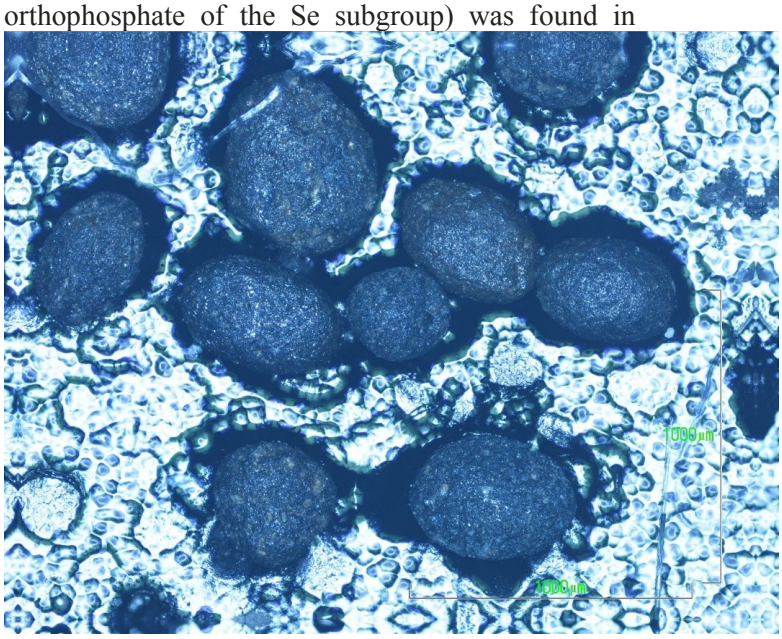

Fig. 1. Microconcretions of cularite under an electron microscope**.**

The studies were carried out at an accelerating voltage of 20 kV. The current of absorbed electrons on the reference cobalt (Co) sample was 200 n Å. The size of the electron probe on the sample surface was 157 nm.

Research results. Using microprobe analysis, we analyzed more than 20 samples and found that in the mineral with an increased amount of silica (more than 3.6 wt. %) there is a direct correlation between the ThO_2 and SiO_2 contents (Table 1).

Table 1. Average statistical content in percentage of SiO_2 and ThO_2 according to microprobe analysis data in terms of 1 formula unit. The numbers indicate the sample numbers.

№	SiO_2	ThO_2
1	50	50
2	49	50
3	50	49
4	50	50
5	49	50
6	48	50
7	49	50
8	50	50
9	50	50
10	50	49
11	49	50
12	49	50
13	50	50
14	50	50
15	50	49
16	50	50
17	49	50
18	50	50
19	49	50
20	50	50

This circumstance gives grounds to assert that an independent phase of $ThSiO_4$ is formed in the form of hattonite. Thus, the actual microconcretions of kularite are polycrystals. Hattonite crystallizes in the monoclinic syngony, which makes it possible to easily enter into an identical structure, such as kularite. It is important to note that the parameters of the unit cells of both minerals are almost identical. Thus, for kularite a=6.77Å, b=7.04 Å, c=6.46 Å, and for hattonite a=6.77Å, b=6.96Å, c=6.49Å, respectively (Pabst at. al., 1951). The similarity of the space groups and parameters of the unit cells allows us to speak about the isotypic nature of these compounds. Since hattonite is a higher temperature mineral than its analogue thorite and crystallizes in the tetragonal syngony, we can talk about higher parameters of kularite formation. Consequently, we can assume a magmatic origin of kularite.

Conclusions.

It is obvious that both the zoning of most of the studied samples and the formation of microconcretions are associated with the simultaneous crystallization of both minerals - kularite and hattonite, and phosphorus-containing black shale strata serve as an effective geochemical barrier on which magmatic hydrothermal solutions are discharged with the formation of rare earth mineralization.

This study is fulfilled under Research program № FMUF 2022-0003 of the Korzhinski Institute of Experimental Mineralogy.

References:

1. Некрасов И.Я, Некрасова Р.А. Генетические особенности куларита // Доклады Академии Наук. – 1995. - Т.344. - №1. - С. 87-90.
2. Некрасова Р.А. Новые данные о составе фосфатной матрицы куларита // Доклады Академии Наук. – 1990. - Т.312. - №2. - С. 464-467.
3. Некрасова Р.А, Некрасов И.Я. Куларит-аутигенная разновидность монацита // Доклады Академии Наук. -1982. - Т. 268. - №3. - С. 688-692.
4. Pabst, Adolf, Hutton,C.O. Yuttonite. A new monoclinic thorium silicate / American Mineralogist. – 1951. – V.36. -_ P. 60-69.

Redkin A.F., Kotova N.P., Nekrasov A.N. Features of the interaction of NaF with niobium oxide compounds in hydrothermal solutions.

Korzhinskii Institute of Experimental Mineralogy RAS
redkin@iem.ac.ru; kotova@iem.ac.ru; alex@iem.ac.ru

Abstract. The interaction of Nb_2O_5 with NaF solutions at 300–900°C, and a pressure of 1–2 kb, in a reducing environment (Ni-NiO, Co-CoO) leads to the formation of nonstoichiometric compounds – oxifluoride Na-Nb bronzes. At 300–550°C, 1 kb, cubic pyrochlore-like ($Fd\bar{3}m$) phases of the composition $Na_{1.5}Nb_2O_5F_{1.1}$ are formed with LC a=10.504(4) Å. At 800 and 900°C, 2 kb, phases of the composition $Na_{0.13}Ca_{0.01}NbO_{2.5}F_{0.115}$ and $Na_{0.24}Ca_{0.00}NbO_{2.5}F_{0.115}$ are formed, presumably of a tetragonal structure, represented by elongated (>100 microns) crystals.

***Keywords**: experiment, pyrochlore-like phases, Raman spectroscopy*

When a mixture of pyrochlore composition containing a deficiency of CaO, NaF+(1-x)CaO+ Nb_2O_5 and Nb_2O_5 interacted with 1 *m*NaCl solution, new phases of the composition $Na_{1-x}NbO_{2.5}F_{1-x-y}$ were obtained. X-ray phase analysis of the experimental products showed that "The Powder Diffraction File (PDF) database contains no information about the obtained compounds". At 800 and 900°C, newly formed crystals were in a mixture with pyrochlore ($CaNaNb_2O_6F$) and were represented by elongated (>100 μm) crystals (Fig. 1, 2).

The experimental products were pressed into polystyrene, polished, and then chemically analyzed. It was found that small octahedral crystals are represented by pyrochlore, of almost ideal composition, with the unit cell parameter a=10.42(1) Å (Redkin et al., 2013), while elongated crystals obtained at 800°C have the composition $Na_{0.13}Ca_{0.01}NbO_{2.5}F_{0.115}$ (11 measurements), and at 900°C – $Na_{0.24}Ca_{0.00}NbO_{2.5}F_{0.115}$ (15 measurements).

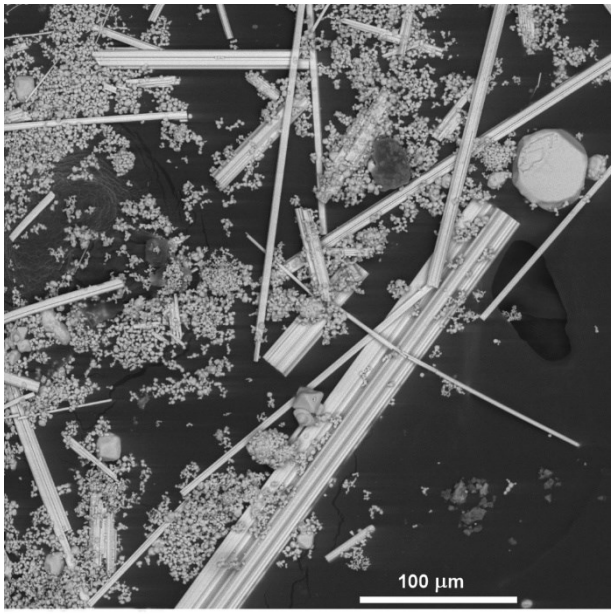

Fig. 1. SEM image of the run products on the synthesis of pyrochlore $NaCaNb_2O_6F$ at 800 °C, a pressure of 2 kbar, 1.0 *m*NaF.

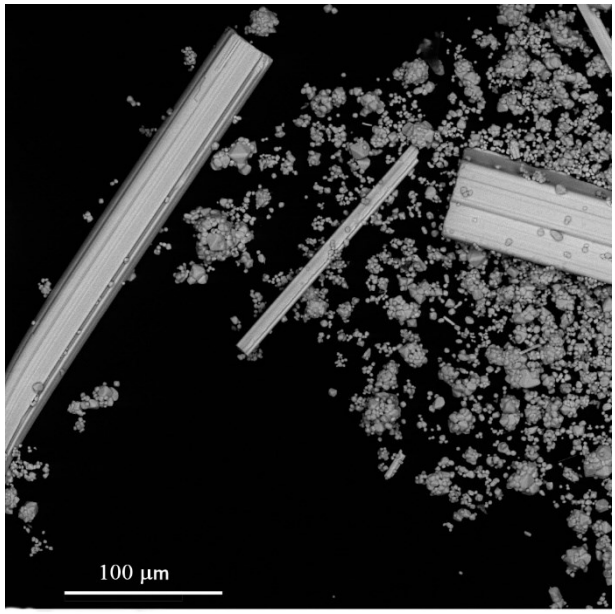

Fig. 2. SEM image of the run products on the synthesis of pyrochlore $NaCaNb_2O_6F$ at 900 °C, a pressure of 2 kbar, 1.0 *m*NaF.

X-ray diffraction patterns of newly formed crystalline phases at 800 and 900°C, despite their external similarity (Fig. 3), differ significantly. If we assume that both phases have a tetragonal structure typical of tungsten bronzes (Ribnick et al., 1963), then they correspond to the lattice constants (LC) equal to for the experiment at 800 °C: a = 5.24, c = 23.886 Å, V = 655.8 Å^3; and for the experiment at 900 °C – a = 23.404, c = 3.939 Å, V=2158 Å^3.

X-ray diffraction patterns of phases obtained at 300–550°C, 1 kb, Co-CoO buffer (Fig. 4) back in 2016 (Kotova, 2017) were not identified then. When analyzing the XRD spectrum, it was found that all newly formed phases have the chemical composition $Na_{1.5}Nb_2O_5F_{1.1}$, a pyrochlore structure ($Fd\bar{3}m$) with lattice constant (LC) equal to 10.504(4) Å. The run products are represented by well-formed octahedral crystals (Fig. 5) – typical for pyrochlore. The product yield is 100%. A similar pyrochlore structure was first described in the work (Boivin et al., 2022). According to their data, the fine-crystalline phase (≤ 1 μm), obtained by hydrothermal synthesis from Nb_2O_5 at 240°C in 0.02 *m*NaF, had the composition $Na_2Nb_2O_5F_2$ with a LC = 10.5181(3) Å.

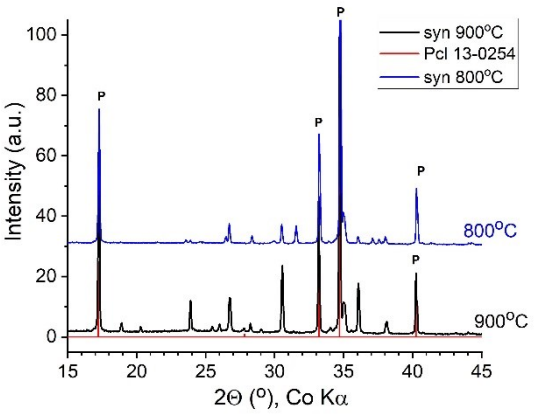

Fig. 3. XRD of newly formed phases in runs at 800–900°C, a pressure of 2 kbar, 1.0 *m*NaF. Pyrochlore standard (Pcl) PDF13-0254

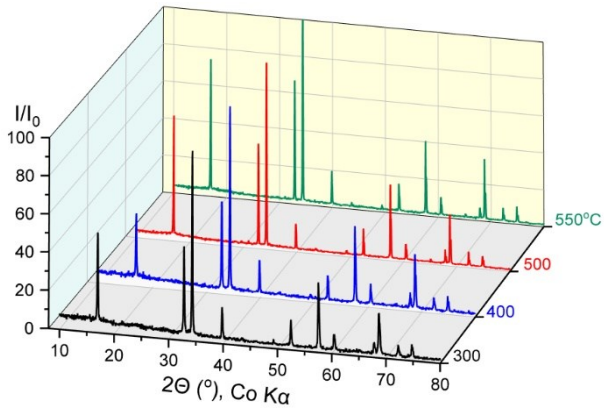

Fig. 4. 3D XRD of newly formed phases in Nb_2O_5 solubility runs at 300–550°C, a pressure of 1 kbar, 1.0 *m*NaF..

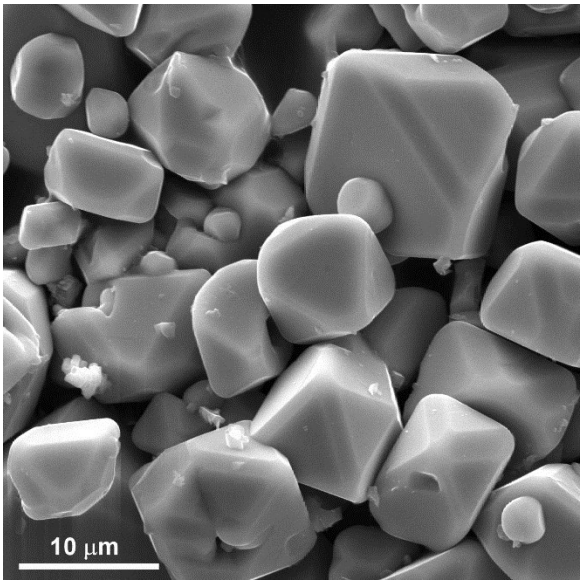

Fig. 5. SEM image of the run products on Nb_2O_5 solubility at 550°C, a pressure of 1 kbar, 1.0 *m*NaF, Co-CoO buffer.

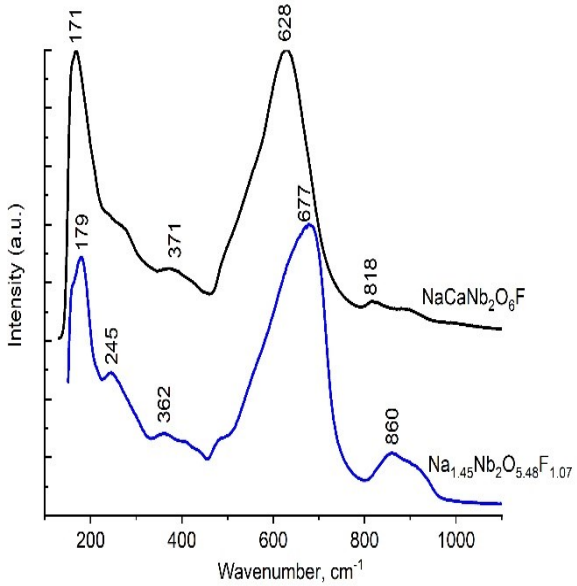

Fig. 6. Raman spectra of Pcl and $Na_{1.45}Nb_2O_{5.48}F_{1.07}$ – of the run products on the solubility of Nb_2O_5 at 550°C, a pressure of 1 kbar, 1.0 *m*NaF, Co-CoO buffer.

The newly formed pyrochlore-like phase from the experiment at 550°C was studied by Raman spectroscopy (RS) on a Renishaw (RM1000) instrument equipped with a Leica microscope (NPPhMIV IEM RAS) (Fig. 6).

Synthetic pyrochlore of the composition $CaNaNb_2O_6F$ was used as a comparison standard. Analysis of the spectra indicates that the compounds under study have great similarity.

The conducted studies indicate that the interaction of Nb_2O_5 with NaF solutions at 300–800°C and a pressure of 1–2 kbar, in a reducing environment (Ni-NiO, Co-CoO buffers) leads to the formation of non-stoichiometric compounds – oxyfluoride Na-Nb bronzes:

$0.5Nb_2O_5 + (1\text{-}x)NaF + 0.5yH_2 \rightarrow Na_{1-x}Nb(O_{2.5}F_{0.5})F_{0.5-y-x} + yHF.$

As a result of this reaction, free hydrofluoric acid is released, and the acidity of the hydrothermal solution changes. The *T-P-f*O_2 parameters and pH of the solution ultimately determine the chemical composition and crystal structure of the newly formed phases. At 300–550°C, 1 kbar cubic pyrochlore-like ($Fd\bar{3}m$) phases of the composition ~ $Na_{1.5}Nb_2O_5F_{1.1}$ with the LC a=10.504(4). Å are formed. At 800°C and 900°C, 2 kbar phases of the composition $Na_{0.13}Ca_{0.01}NbO_{2.5}F_{0.115}$ and $Na_{0.24}Ca_{0.00}NbO_{2.5}F_{0.115}$ are formed, presumably of tetragonal structure 1 and 2, represented by elongated (>100 μm) crystals.

The work was carried out with the financial support of the Russian Federation project represented by the Ministry of Education and Science of Russia, No. 13.1902.24.44, agreement No. 075-15-2024-641.

The authors are grateful to ***N.A. Drozhzhina*** *(IEM RAS)* ***and O.L. Samokhvalova*** *for assistance in conducting X-ray analyses of solid experimental products, and to O.V. Reutova for assessing of the LC parameters of newly formed phases.*

References

Boivin E., Pourpoint F., Saitzek S., Simon P., Roussel P, Kabbour H. An unusual O^{2-}/F^{-} distribution in the new pyrochlore oxyfluorides: $Na_2B_2O_5F_2$ (B = Nb, Ta) // Chemical Communications. 2022. V. 58(14). P. 2391-2394.

Kotova N.P. Experimental study of temperature influence on niobium oxide solubility in NaF and LiF solution // Experiment in Geosciences 2017. V. 23. No 1. P. 107–108.

Redkin A.F., Ionov A.M., Kotova N.P. Hydrothermal synthesis of pyrochlores and their characterization // Phys. Chem. Miner. 2013. V. 40. P. 733–745.

Ribnick A.S., Post B., Banks E. Phase transitions in sodium tungsten bronzes. In Nonstoichiometric Compounds // Am. Chem. Soc. 1963. 39. P. 246-253.